Influence of domain wall anisotropy on the current-induced hysteresis loop shift for quantification of the Dzyaloshinskii-Moriya interaction

Takaaki Dohi,[1,2] Shunsuke Fukami,[1,3,4,5,6,*] and Hideo Ohno[1,3,4,5,6]
[1]*Laboratory for Nanoelectronics and Spintronics, Research Institute of Electrical Communication, Tohoku University, Sendai 980–8577, Japan*
[2]*Institut für Physik, Johannes Gutenberg-Universität Mainz, Staudingerweg 7, 55128 Mainz, Germany*
[3]*Center for Science and Innovation in Spintronics, Tohoku University, 2-1-1 Katahira, Aoba, Sendai 980–8577, Japan*
[4]*Center for Spintronics Research Network, Tohoku University, 2-1-1 Katahira, Aoba-ku, Sendai 980–8577, Japan*
[5]*Center for Innovative Integrated Electronic Systems, Tohoku University, 468-1 Aramaki Aza Aoba, Aoba-ku, Sendai 980–0845, Japan*
[6]*WPI-Advanced Institute for Materials Research, Tohoku University, 2-1-1 Katahira, Aoba-ku, Sendai 980–8577, Japan*

(Received 9 April 2021; revised 5 June 2021; accepted 16 June 2021; published 29 June 2021)

Using several material systems with various magnitudes of the interfacial Dzyaloshinskii-Moriya interaction (DMI), we elucidate a critical influence of domain wall (DW) anisotropy on the current-induced hysteresis loop shift scheme widely employed to determine the magnitude of the Dzyaloshinskii-Moriya effective field (H_{DMI}). Taking into account the DW anisotropy in the analysis of the hysteresis loop shift, which has not been included in the original model [Phys. Rev. B **93**, 144409 (2016)], we show that it provides quantitative agreement of H_{DMI} with that determined from an asymmetric bubble expansion technique for small DMI material systems. For large DMI systems, the DW anisotropy gives rise to nonlinearity in the response of spin-orbit torque efficiency to the in-plane magnetic field, from which H_{DMI} can be determined. The consequence of the directions of DW motion in the Hall device on the current-induced shift of the hysteresis loop is also discussed. The present findings deliver important insights for reliable evaluation of DMI, which are of significance in spintronics with chiral objects.

DOI: 10.1103/PhysRevB.103.214450

I. INTRODUCTION

The Dzyaloshinskii-Moriya interaction (DMI) [1,2] is known to stabilize various chiral spin textures such as Néel domain wall (DW) [3–6] and magnetic skyrmion [7–10]. These chiral objects are expected to function as a key ingredient in various emerging spintronic technologies, e.g., DW devices [11–13], neuromorphic computing [14,15], and so on [16–19], leading to creation of a new paradigm of spintronics [20–22]. Furthermore, unconventional bulklike DMI [23] and interlayer DMI [24,25] have been recently found, which are expected to invigorate the field with the capability to realize topological spin textures not only in one (1D) or two-dimensional (2D) but also in three-dimensional (3D) spaces [26]. In these regards, easily accessible yet reliable evaluation of DMI is in great demand.

Methods to quantify the DMI developed so far roughly fall into two categories; one utilizes DW [27–33] and the other relies on spin-wave propagation [34–36]. The former is further classified into two subcategories based on the focused phenomenon. The first one has been known as the asymmetric magnetic bubble expansion scheme, where one observes magnetic bubble expansion under in-plane magnetic field ($H_{x,y}$), typically using magneto-optical Kerr effect (MOKE) microscopes and captures the modification of the DW velocity (υ_{DW}) [27,28,30]. DMI inherently acts as an effective field, so-called DMI effective field (H_{DMI}), for the DWs, and applying $H_{x,y}$ lifts the degeneracy between the up-to-down ($\uparrow\downarrow$) and down-to-up ($\downarrow\uparrow$) DW energies. Consequently, the bubble shows an asymmetric expansion under $H_{x,y}$, from which sign and magnitude of DMI can be determined. The second subcategory makes use of the modification of current-induced spin-orbit torque (SOT) efficiency (χ_{SOT}) acting on DWs that changes with the degree of chirality of the DWs [3,29,32,37–39]. Nonequilibrium spins accumulated via spin-orbit interaction-related phenomena in systems with broken space inversion symmetry [40–42] generates SOT which serves as an effective magnetic field (H_{eff}) driving DWs. Since χ_{SOT} depends on H_{DMI} and $H_{x,y}$ via the degree of chirality, $H_{x,y}$ dependence of χ_{SOT} allows one to quantify H_{DMI}. In practice, magneto-optical or electrical means have been employed to measure the modification of χ_{SOT} under $H_{x,y}$. The former mainly utilizes MOKE microscope and observes υ_{DW} [29,38] or depinning field shift [3,37,39]. Recent studies confirmed an agreement of the obtained H_{DMI} with that determined from the asymmetric bubble expansion or spin-wave schemes [43,44]. On the other hand, for the electrical means, the main focus of this work, originally proposed by Pai *et al.* [32], one measures a current-induced shift of hysteresis loop through the anomalous Hall effect (known as the current-induced hysteresis loop shift scheme). Although this technique is the most widely utilized [45–51] mainly because it does not require any nanofabrication processes and specific apparatus (e.g., MOKE microscope and laser systems with a well-defined wave vector), there remain some open questions. For instance,

*s-fukami@riec.tohoku.ac.jp

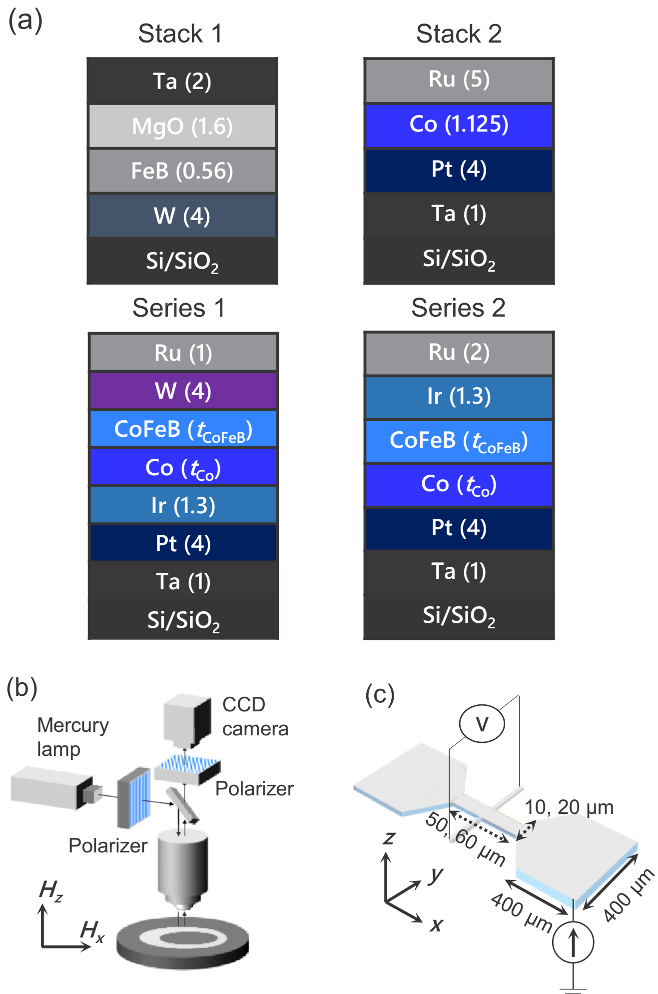

FIG. 1. (a) Stack structures. (b) Experimental setup for asymmetric magnetic bubble expansion scheme, and (c) setup and device structure for current-induced hysteresis loop shift scheme.

this scheme tends to indicate larger H_{DMI} than that with other schemes [52] whose reason has not been clarified. Also, some material systems show nonlinear behavior of χ_{SOT} against $H_{x,y}$ even though it has not been explicitly pointed out [10,45,51], and this behavior was not described in the original model [32]. Moreover, while the DW could in reality move in 2D space, the model for the analysis assumes one direction along the wire and the consequence of 2D DW motion has been unclear.

Here, we address these unsolved issues of the current-induced hysteresis loop shift scheme by testing several material systems with various magnitudes of DMI. DMI is also quantified by two independent techniques; observation of asymmetric magnetic bubble expansion (Sec. II) and analysis of coercivity under out-of-plane and in-plane fields with the droplet model [33,53] (Appendix). We revisit the procedure of analysis [54] and show that some anomalies in the results of the hysteresis loop shift can be explained by considering the effect of DW anisotropy.

II. SAMPLE STRUCTURE AND MEASUREMENT SETUP

In this study, we investigate four kinds of stack structures, stack 1, stack 2, series 1, and series 2, shown in Fig. 1(a), which were used in our previous works [10,52]. Stack structures of each system are as follows: sub./ W(4)/ $Fe_{75}B_{25}$(0.56)/ MgO(1.6)/ Ta(2) [stack 1], sub./ Ta(1)/ Pt(4)/ Co(1.125)/ Ru(5) [stack 2], sub./ Ta(1)/ Pt(4)/ Ir(1.3)/ Co(t_{Co})/ $Co_{19}Fe_{56}B_{25}$(t_{CoFeB})/ W(4)/ Ru(1) [series 1], sub./ Ta(1)/ Pt(4)/ Co(t_{Co})/ $Co_{19}Fe_{56}B_{25}$(t_{CoFeB})/ Ir(1.3)/ Ru(2) [series 2], where the numbers in parentheses denote nominal thickness in nm. According to our previous studies [10,52], the stack 1 and series 1 represent a small-DMI and intermediate-DMI systems, respectively, whereas the stack 2 and series 2 fall into large-DMI systems. All the stacks are deposited by dc and rf magnetron sputtering on thermally oxidized Si substrates. After the deposition, only the stack 1 is annealed at 300 °C for 1 h to induce interfacial perpendicular magnetic anisotropy. Figures 1(b) and 1(c) show the experimental setup for asymmetric magnetic bubble expansion and current-induced hysteresis loop shift measurements, respectively. For the latter, we process all the stacks into 50 or 60-μm-long and 10 or 20-μm-wide Hall-bar devices with a large reservoir for domain nucleation, using photolithography and Ar-ion milling. Magnetization measurement is performed to evaluate the spontaneous magnetization M_{S} and effective magnetic anisotropy energy density K_{eff}. We find that all the stacks have perpendicular magnetization easy axis.

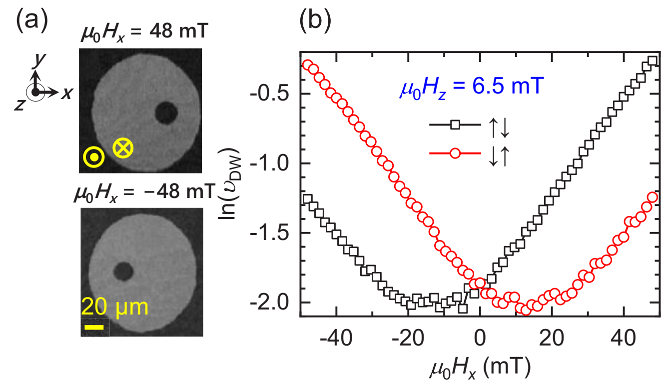

FIG. 2. Asymmetric magnetic bubble expansion in stack 1 studied in Ref. [52]. (a) MOKE images for asymmetric bubble expansion under $\mu_0 H_x = \pm 48$ mT, where $\odot$ and $\otimes$ denote up and down magnetic domains, respectively. (b) H_x dependence of υ_{DW}, where black and red plots denote the result for ↑↓ and ↓↑ DWs, respectively.

III. RESULTS

A. Asymmetric magnetic bubble expansion

We first show the results of asymmetric magnetic bubble expansion in stack 1. The measurement starts from nucleating the bubble domain by applying pulsed perpendicular magnetic field H_z. After that, we observe a bubble expansion under a simultaneous application of static H_x and pulsed H_z and extract υ_{DW}. Figure 2(a) shows a typical MOKE image of the bubble expansion under H_x. Asymmetry is clearly observed, indicating a presence of DMI with a right-handed/clockwise chirality, consistent with previous works [55,56]. Figure 2(b) shows H_x dependence of υ_{DW} for ↑↓ and ↓↑ DWs. Antisymmetric contribution to υ_{DW}, which hinders precise evaluation of DMI [38,43,57], is not seen, indicating that the applied field, $\mu_0 H_z = 6.5\,\mathrm{mT}$ (μ_0 is permeability in free space), is large enough that DW moves in depinning or flow regimes and H_{DMI} can be determined from this result. The dependence shows clear symmetric behavior with minimum v_{DW} at finite H_x, where DW is expected to form Bloch-type configuration due to the cancelation of H_{DMI} by H_x [27,54,58]. Consequently, H_{DMI} is determined from the minima as $\mu_0 H_{\mathrm{DMI}} = 13 \pm 5\,\mathrm{mT}$.

B. Current-induced hysteresis loop shift for small DMI system

We next perform the current-induced hysteresis loop shift measurement for stack 1. As mentioned earlier, current injected into heterostructures with sizable spin-orbit coupling generates H_{eff} acting on DWs whose magnitude and direction vary with the direction of the magnetic moment inside DW. In the case of current flowing in the x direction as shown in Fig. 1(c), H_{eff} along the z direction is given by [32]

$$\mu_0 H_{\mathrm{eff}} = \chi_{\mathrm{SOT}} J, \qquad \chi_{\mathrm{SOT}} = \chi'_{\mathrm{SOT}}(\cos\varphi_{\uparrow\downarrow} + \cos\varphi_{\downarrow\uparrow})/2, \tag{1}$$

where J denotes current density, χ_{SOT} corresponds to a DW-profile-dependent efficiency of Slonczewski-like SOT [37,54,59], $\varphi_{\uparrow\downarrow/\downarrow\uparrow}$ represents an angle of magnetic moment in the $\uparrow\downarrow/\downarrow\uparrow$ DW measured from the normal direction to the DW plane as depicted in Fig. 3(a). χ'_{SOT} denotes the efficiency of Slonczewski-like SOT, referred to as the effective spin Hall angle for systems where the spin Hall effect is dominant. As can be understood from Eq. (1), $H_{\mathrm{eff}} = 0$ at zero H_x because $\varphi_{\uparrow\downarrow} = \varphi_{\downarrow\uparrow} + \pi$, where $\uparrow\downarrow$ and $\downarrow\uparrow$ DWs concurrently move in the same direction [4,5]. Upon increasing H_x that breaks the chiral Néel wall configuration, H_{eff} becomes finite, leading to the shift of hysteresis loop, and the shift linearly increases with the applied dc current I through the increase in SOT.

Figure 3(b) shows a typical example of the hysteresis loop shift; anomalous Hall resistance R_{AHE} vs H_z at $\mu_0 H_x = 50\,\mathrm{mT}$ and $I = \pm 15\,\mathrm{mA}$. The magnitude of the shift (H_{eff}) can be determined from the peak of the derivative. Figure 3(c) shows H_{eff} as a function of I. A linear relation in accordance with Eq. (1) is confirmed, indicating that H_{eff} arises from SOT and χ_{SOT} is obtained from the slope. Figure 3(d) shows χ_{SOT} as a function of $H_{x,y}$. $|\chi_{\mathrm{SOT}}|$ increases with H_x whereas it remains around zero for all the measured H_y, also consistent with Eq. (1). According to the original model [32], H_{DMI} can be approximated by the in-plane field along the longitudinal direction $H_x^{\max}$ at which all the DW moments align in the x direction and χ_{SOT} is maximized [rightmost cartoon in Fig. 3(a)]. However, $\mu_0 H_x^{\max}(=\mu_0 H_{\mathrm{DMI}})$ is about 35 mT, which is about twice as large as that determined from the asymmetric magnetic bubble expansion scheme mentioned earlier (13 ± 5 mT).

It is expected that the large H_{DMI} obtained in the current-induced hysteresis loop shift scheme stems from the contribution of DW anisotropy, which is naturally included in the analysis of bubble expansion but is not in the hysteresis loop shift scheme. As depicted in Fig. 3(a), DWs change their configuration between Néel and Bloch types under H_x. Considering the contribution of DW anisotropy that inherently favors the Bloch-type configuration in thin films with a perpendicular easy axis, for systems with finite

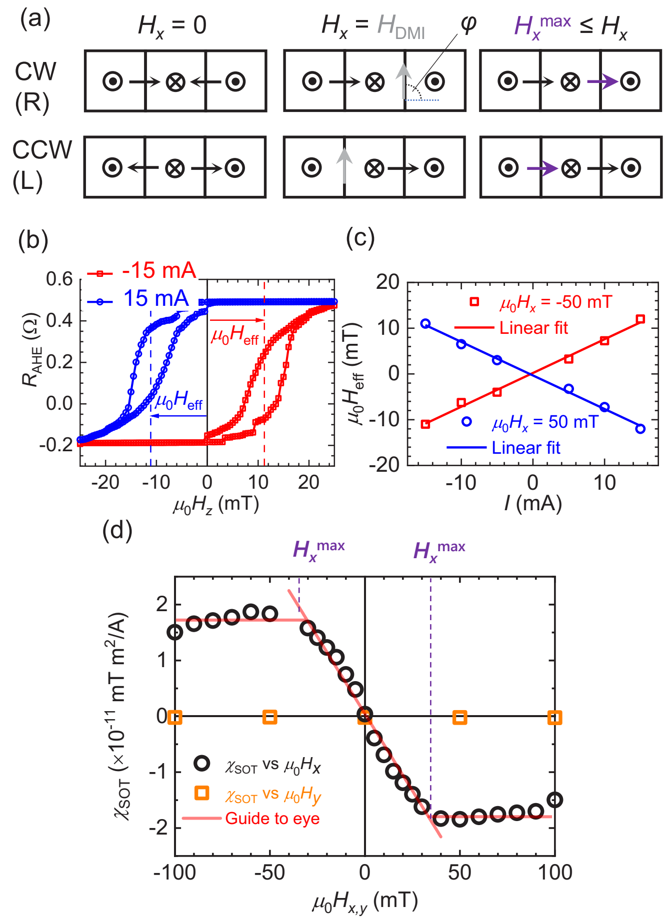

FIG. 3. Current-induced hysteresis loop shift measurement in stack 1 studied in Ref. [52]. (a) Schematics of modification of clockwise (CW)/ right-handed (R) and counterclockwise (CCW)/ left-handed (L) DW configurations under H_x. Arrows denote DW moments, φ the relative angle of DW moment from DW plane, and $H_x^{\max}$ the H_x to saturate χ_{SOT}. (b) Current-induced hysteresis loop shift under $\mu_0 H_x = 50\,\mathrm{mT}$, where red and blue symbols correspond to results at $I = -15$ and 15 mA, respectively. (c) H_{eff} as a function of I, where red and blue symbols represent the results at $\mu_0 H_x = -50$ and 50 mT. (d) In-plane field dependence of χ_{SOT} where plots in black and orange denote the results under H_x and H_y.

DMI, DWs should form chiral Néel-type configuration at $H_x = 0$, Bloch-type configuration at $H_x = H_{\mathrm{DMI}}$, and nonchiral Néel-type configuration at $H_x\ (= H_x^{\max}) = H_{\mathrm{DMI}} + H_{\mathrm{S}}$, as depicted in the left, center, and right cartoons in Fig. 3(a), respectively. Here, H_{S} denotes DW anisotropy field given as $H_{\mathrm{S}} = 4K_{\mathrm{D}}/\pi M_{\mathrm{S}}$ [27,38,54,58], where K_{D} approximated by $\ln(2)M_{\mathrm{S}}^2 t/(2\pi\mu_0\delta)$ [60] indicates the DW anisotropy energy density (t and δ are ferromagnetic layer thickness and DW width, respectively). Therefore, by considering the effect of DW anisotropy, H_{DMI} should be given by $H_{\mathrm{DMI}} = H_x^{\max} – H_{\mathrm{S}} (\neq H_x^{\max})$. We calculate $\mu_0 H_{\mathrm{S}}$ to be 25 ± 5 mT using $M_{\mathrm{S}} = 1.75\,\mathrm{T}$, $K_{\mathrm{eff}} t = 0.23\mathrm{mJ/m^2}$, $t = 0.56\,\mathrm{nm}$, and $A_{\mathrm{S}} = 8$–$20\,\mathrm{pJ/m}$, leading to $\mu_0 H_{\mathrm{DMI}} = 10 \pm 5\,\mathrm{mT}$ (M_{S} and K_{eff} are determined from a magnetization-curve measurement [52] and the range of exchange stiffness constant A_{S} is determined on the basis of previous observations [61–66] considering its dependence on thickness [61], annealing temperature [62], composition of ferromagnet [63], etc.). The obtained H_{DMI} agrees well with that determined from the asymmetric bubble expansion scheme. We note that the correction of H_{S} is especially important for small DMI systems because, in that case, $\varphi_{\uparrow\downarrow/\downarrow\uparrow}$ is not necessarily 0 or π at $H_x = 0$.

C. Intermediate and large DMI material systems

Next, we investigate the series 1, 2, and stack 2, which have intermediate to large H_{DMI} compared with the DW anisotropy field [10]. Figure 4(a) shows the H_x dependence of χ_{SOT} in series 1 that represent the intermediate DMI system. Intriguingly, nonlinearity appears with the change in the thickness of Co and CoFeB layers. Such nonlinear behavior disables the determination of H_{DMI} based on the original model [32] as well as the modified model described above but has been actually observed in several previous works although it has not been pointed out [45,51]. The observed nonlinearity is expected to relate to the magnitude of DMI because it becomes apparent with increase/decrease in the Co/CoFeB thickness which is known to be accompanied by the increase in the magnitude of interfacial DMI according to previous studies [10,56]. Figures 4(b) and 4(c) show R_{AHE}-H_z loops at $\mu_0 H_x = 150$ and 350 mT for stack 2 representing a large DMI system; minuscule (significant) shift is observed at $\mu_0 H_x = 150$ mT (350 mT), unlike stack 1 with small DMI. Figure 4(d) summarizes χ_{SOT} vs H_x for stack 2 and series 2, where the nonlinearity is more evident than the series 1.

This anomaly can be also explained by considering the contribution of DW anisotropy as follows. For large DMI systems, as depicted in Fig. 4(e), one can expect that DWs maintain the chiral Néel-type configuration until a certain H_x ($=H_x^{\min}$), above which they gradually transform to the Bloch-type configuration until $H_x = H_{\mathrm{DMI}}$ and then to the nonchiral Néel-type configuration until $H_x = H_x^{\max} = H_{\mathrm{DMI}} + H_{\mathrm{S}}$, where H_x overcomes H_{S} and H_{DMI}. In other words, $\varphi_{\uparrow\downarrow/\downarrow\uparrow}$ changes only in the field range from $H_x^{\min} = H_{\mathrm{DMI}} - H_{\mathrm{S}}$ to $H_x^{\max} = H_{\mathrm{DMI}} + H_{\mathrm{S}}$. Accordingly, H_{S} and H_{DMI} can be obtained by $H_{\mathrm{S}} = (H_x^{\max} - H_x^{\min})/2$ and $H_{\mathrm{DMI}} = (H_x^{\max} + H_x^{\min})/2$, respectively. Following these relations, we determine $\mu_0 H_{\mathrm{S}}$ to be 85–100 mT for both stack 2 and series 2, and $\mu_0 H_{\mathrm{DMI}}$ to be 200 mT (series 2) and 300 mT (stack 2). These values agree well with that determined from an analysis of coercivity under out-of-plane and in-plane fields based on the droplet model [33,53] (Appendix) and previous MOKE-based measurements [28,38,67], indicating the validity of the modified model.

IV. EFFECT OF DIMENSIONALITY

As described above, we find that inclusion of DW anisotropy is crucial to quantify the DMI irrespective of its magnitude. In particular, for large DMI systems, DW anisotropy gives rise to an anomalous nonlinear variation of the SOT efficiency with the in-plane field. Here, one question arises, that is, why the nonlinear behavior was not observed in the original work although the studied stacks (Pt/Co/MgO or Ta) are expected to fall into the large DMI family [32]. In the following, we describe that the dimensionality of the DW motion in the studied device is a clue to solve this question, and

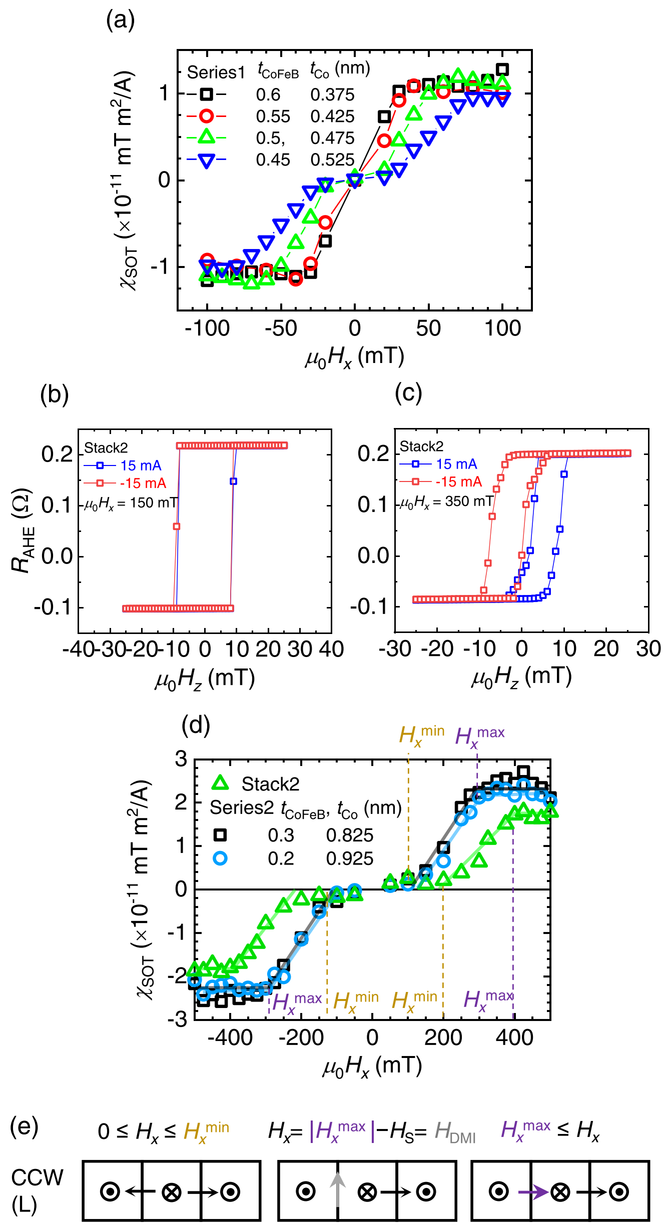

FIG. 4. Current-induced hysteresis loop shift measurement in series 1, 2 and stack 2. (a) H_x dependence of χ_{SOT} for series 1 where black, red, green, and blue symbol denote for (t_{Co}, t_{CoFeB}) (0.375, 0.60), (0.425, 0.55), (0.475, 0.50), and (0.525, 0.45) nm, respectively. Current-induced hysteresis loop shift under (b) $\mu_0 H_x = 150$ mT and (c) 350 mT, where blue and red symbols correspond to $I = 15$ and -15 mA, respectively. (d) H_x dependence of χ_{SOT} in stack 2 and series 2, where green, black, and sky-blue symbols correspond to stack 2, (t_{Co}, t_{CoFeB}) = (0.30, 0.825), (0.20, 0.925) nm of series 2, respectively. (e) Schematics of modification of counterclockwise (CCW)/left-handed (L) DW configuration under H_x for large DMI material system.

1D motion of DW along the current direction is a prerequisite to apply the analysis scheme for the hysteresis loop shift.

According to a previously conducted MOKE observation of magnetization reversal process under SOT and H_x, where a virtually linear dependence of χ_{SOT} was reported [32,46,49], domain is initially nucleated near the wire edge due to the

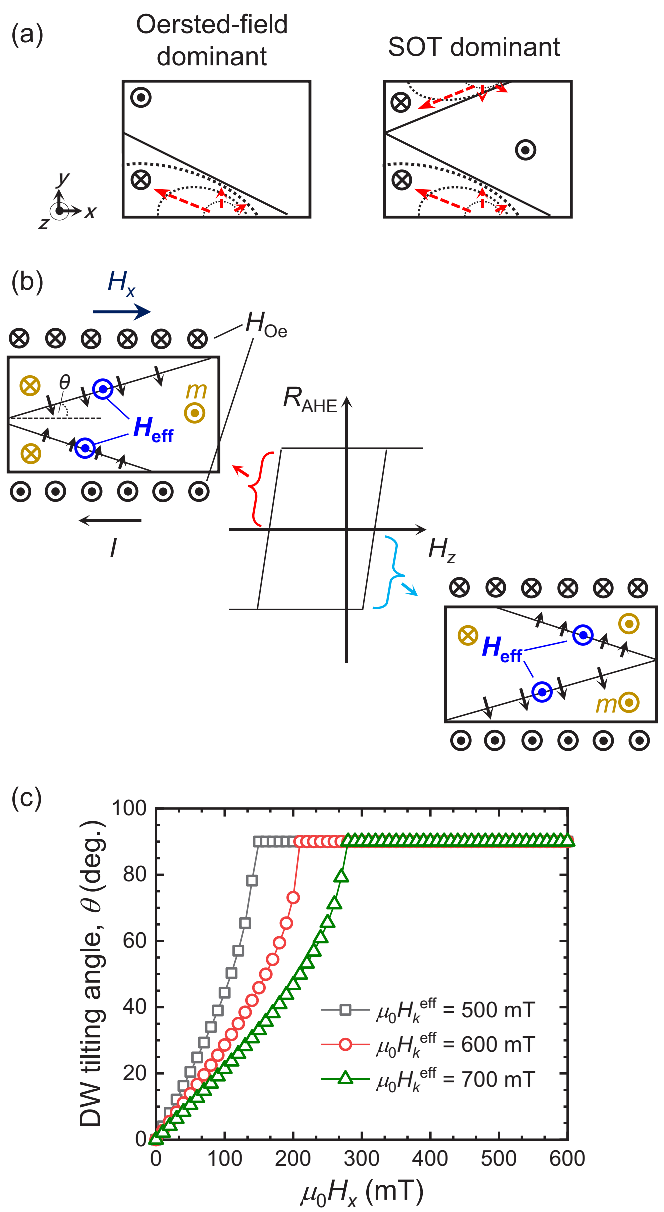

FIG. 5. (a) Schematics of domain nucleation and asymmetric expansion with current injection under H_x for Oersted-field dominant (left) and SOT dominant (right) cases [46]. (b) Schematic illustration of the impact of DW motion in the y direction on hysteresis loop shift. H_{eff} and θ denote current-induced effective field acting on DW and tilting angle of DW plane, respectively. (c) Calculated H_x dependence of θ by Eq. (2), where black, red, and green symbols denote the calculation results for the effective anisotropy field of $\mu_0 H_k^{\mathrm{eff}} = 500$, 600, and 700 mT, respectively. The following magnetic parameters are used for calculation; $M_S = 1.7$ T, $t = 1.125$ nm, $A_S = 10$ pJ/m.

Oersted field [68] and/or the SOTs [46]. Subsequently, DW displaces not only in the x but also in the y directions owing to a large-sized device with a low aspect ratio [32,46] . To examine the influence of DW motion in the y direction, we consider a magnetization reversal process brought about by sweeping H_z under static H_x and I in a relatively wide wire with a large DMI. As illustrated in Fig. 5(a), magnetic domains are nucleated at the wire edge under H_x, where nucleation starts from both edges (either of edges) if SOT (Oersted field) is dominant [46]. Then, H_x forces the magnetization inside the DW to point to the x direction, eventually causing a tilting of DW plane with an angle θ due to the DMI [69]. At this stage, unlike the case for DWs moving in the x direction, ↑↓ and ↓↑ DWs moving in the y direction feel H_{eff} with the same sign, as depicted in Fig. 5(b). Also, the sign of H_{eff} is the same between up to down and down to up reversal processes, leading to a shift of hysteresis loop. Note that this scenario holds true regardless of the initial nucleation site depicted in Fig. 5(a) as well as the number of nucleated domains.

A notable point here is that H_x dependence of χ_{SOT} can be represented by H_x dependence of θ because χ_{SOT} is proportional to sin θ, where θ is determined by the energy equilibrium in the quasiequilibrium process. For simplicity, we assume that the Néel-type DW configuration, i.e., $\varphi = 0$, is maintained due to a large DMI, and tilting of DW plane is much more dominant than the modification of the internal DW configuration [37,69]. The tilting angle θ of the DW plane at equilibrium is approximated by [69]

$$\begin{aligned} \sin\theta &\approx \gamma_z/\gamma_{\mathrm{DW}}, \\ \gamma_z &= -\pi M_S H_x \delta/\mu_0 \\ \gamma_{\mathrm{DW}} &= 4\sqrt{A_S K_{\mathrm{eff}}} + 2\delta K_D - \pi M_S H_{\mathrm{DMI}}\delta/\mu_0, \end{aligned} \tag{2}$$

where γ_Z represents the Zeeman energy contribution to internal DW energy γ_{DW}. Figure 5(c) shows the H_x dependence of θ calculated for $\mu_0 H_{\mathrm{DMI}} = 200$ mT. A linear dependence is seen except for large H_x regime where Eq. (2) is not applicable [69], accounting for the observed linearity between χ_{SOT} and H_x in the original work with a large DMI systems [32]. We also note that, even in considering the tilting of DW plane for DWs moving in the x direction [37], it cannot account for the observed linearity, indicating that DW motion in the y direction is only the viable explanation. It is notable that, according to Fig. 5(c), the behavior strongly depends on the effective magnetic anisotropy field H_k^{eff}, indicating that magnitude of DMI cannot be determined in a straightforward way, unlike the case of 1D motion along the x direction. We also note that this calculation is consistent with the previously observed H_k^{eff} dependence of $H_x^{\max}$ [32,47].

In our experiments shown in Sec. III C, the reversed domain is nucleated in the large reservoir [Fig. 1(c)] and the direction of DW motion in the wire is effectively limited to the x direction. This fact leads to the nonlinear behavior unlike the original study [32] and allows us to determine H_{DMI} following the 1D model as described in Sec. III C. In other words, if one observes linear behavior of χ_{SOT} and obtains $|H_{\mathrm{DMI}}| > H_S$, it suggests a DW motion in the y direction and determined H_{DMI} does not reflect the correct value. It is noteworthy that all the determined H_{DMI} and H_S well agree with MOKE-based measurements [28,38,67], implying that the tilting of DW plane during the motion in the x direction [37] is insignificant for our devices probably due to a restoring force due to the DW tension relating to the edge condition [70]. We finally note that even without a large reservoir, the corrected analysis described above can be used as long as the DW motion is effectively constrained in the x direction. For example, in the case of a chirality-induced asymmetric magnetic nucleation, DW propagation was reported to take place mainly in the

x direction [53], allowing one to analyze the results with the corrected model.

V. CONCLUSION

We study the effect of DW anisotropy on the current-induced hysteresis loop shift scheme, which is widely used for determining the magnitude of DMI, utilizing several material systems with various magnitudes of DMI. We find that incorporation of DW anisotropy into the model for the analysis is necessary to quantify the DMI effective field H_{DMI}, although the manifestation of DW anisotropy varies with the magnitude of DMI. For small DMI material systems, we find that H_{DMI} can be obtained by subtracting the DW anisotropy field H_{S} from the field $H_x^{\max}$ at which the SOT efficiency χ_{SOT} saturates with respect to the in-plane field H_x. For large DMI systems, a nonlinear H_x dependence of χ_{SOT} appears, from which H_{DMI} can be determined. We also reveal that the nonlinear behavior does not appear even in large DMI systems if the DW is not constrained to move along the current direction and H_{DMI} cannot be accurately determined for such a case. Therefore, the prescription for H_{DMI} determination with the current-induced hysteresis loop shift can be summarized as follows. First, one measures χ_{SOT} vs H_x. If the obtained dependence shows nonlinearity, one should use the large-DMI correction described in Sec. III C. If nonlinearity is not observed, one should tentatively use the small DMI correction described in Sec. III B and quantify H_{S} and H_{DMI}. If $|H_{\mathrm{DMI}}| < H_{\mathrm{S}}$ is satisfied, the obtained H_{DMI} should be reliable; otherwise, one needs to redesign the device or consider employing different methods because the DW motion in the y direction is likely to take place as described in Sec. IV. The present findings unravel the puzzling issues of the current-induced hysteresis loop shift scheme and offer an important insight for reliable quantification of DMI which is crucial for spintronics with chiral objects.

ACKNOWLEDGMENTS

We thank S. DuttaGupta, B. Jinnai, T. Hirata, H. Iwanuma, K. Goto, and C. Igarashi for their technical support and fruitful discussion. A portion of this work was supported by the ImPACT Program of CSTI, JSPS Kakenhi No. 19H05622, and RIEC Cooperative Research Projects.

APPENDIX: CHARACTERIZATION BY REFERENCE METHOD FOR LARGE DMI SYSTEM

Here, we examine the validity of the correction for large DMI systems described in Sec. III C, by measuring the coercivity under in-plane and out-of-plane fields and analyzing with the droplet model [23,33,53,71]. This method focuses on nucleation of magnetic domains rather than DW motion at zero current and considers the modification of DW energy with in-plane magnetic fields. The nucleation field H_{n} of a magnetic cylindrical droplet (bubble) is expressed as [53,72]

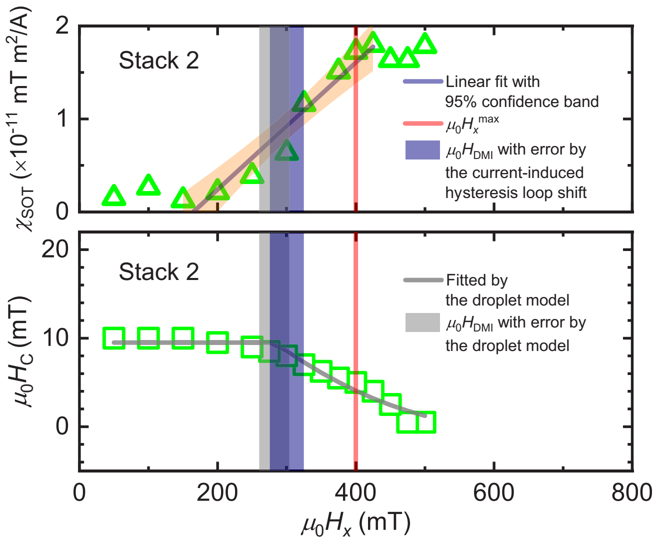

FIG. 6. Comparison of $\mu_0 H_{\mathrm{DMI}}$ determined by the droplet model (bottom) and the current-induced hysteresis loop shift scheme (top) using the stack 2. In the bottom panel (H_{C} vs H_x), grey line and grey-colored area represent the best fit curve by the Eq. (A1) and $\mu_0 H_{\mathrm{DMI}}$ with the uncertain range by the droplet model. In the top panel, navy-blue line and navy-blue-colored area present the linear fit with the orange-colored 95% confidence band and $\mu_0 H_{\mathrm{DMI}}$ with the uncertain range by the current-induced hysteresis loop shift scheme, respectively. The red line corresponds to $\mu_0 H_x^{\max}$ in the current-induced hysteresis loop shift scheme.

$$H_{\mathrm{n}} = \frac{\pi(\gamma'_{\mathrm{DW}})^2 t}{2M_{\mathrm{S}} p k_{\mathrm{B}} T}, \tag{A1}$$

where γ'_{DW}, p, k_{B}, and T are the in-plane magnetic field dependent total DW energy density of the $\uparrow\downarrow$ and $\downarrow\uparrow$ DWs [33,53], the thermal stability factor described in the Néel-Arrhenius law, the Boltzmann constant, and the temperature. The key feature of the expected in-plane field dependence of H_{n} is that H_{n} shows plateau as long as $|H_x| \leqslant |H_{\mathrm{DMI}}|$ due to a constant γ'_{DW} since the $\uparrow\downarrow/\downarrow\uparrow$ DW energies are compensated by each other, whereas H_{n} decreases above the threshold ($|H_x| = |H_{\mathrm{DMI}}|$). Figure 6 shows a comparison of $\mu_0 H_{\mathrm{DMI}}$ determined by the two methods. As can be seen in the bottom panel (droplet model), H_x dependence of coercive field H_{C} is well fitted by Eq. (A1). The grey and navy-blue-colored areas represent $\mu_0 H_{\mathrm{DMI}}$ with uncertain range determined by a fitting based on the droplet model and the current-induced hysteresis loop shift with large DMI correction, respectively. The results from the two methods agree well within the uncertain range, indicating the validity of the correction, whereas $\mu_0 H_x^{\max}$ denoted by the red line, which corresponds to $\mu_0 H_{\mathrm{DMI}}$ in the original model, leads to an overestimation.

[1] I. Dzyaloshinsky, A thermodynamic theory of "weak" ferromagnetism of antiferromagnetics, J. Phys. Chem. Solids **4**, 241 (1958).

[2] T. Moriya, Anisotropic superexchange interaction and weak ferromagnetism, Phys. Rev. **120**, 91 (1960).

[3] P. P. J. Haazen, E. Murè, J. H. Franken, R. Lavrijsen, H. J. M. Swagten, and B. Koopmans, Domain wall depinning governed by the spin Hall effect, Nat. Mater. **12**, 299 (2013).

[4] S. Emori, U. Bauer, S.-M. Ahn, E. Martinez, and G. S. D. Beach, Current-driven dynamics of chiral ferromagnetic domain walls, Nat. Mater. **12**, 611 (2013).

[5] K.-S. Ryu, L. Thomas, S.-H. Yang, and S. Parkin, Chiral spin torque at magnetic domain walls, Nat. Nanotechnol. **8**, 527 (2013).

[6] S.-H. Yang, K.-S. Ryu, and S. Parkin, Domain-wall velocities of up to 750 m s^{-1} driven by exchange-coupling torque in synthetic antiferromagnets, Nat. Nanotechnol. **10**, 221 (2015).

[7] S. Heinze, K. von Bergmann, M. Menzel, J. Brede, A. Kubetzka, R. Wiesendanger, G. Bihlmayer, and S. Blügel, Spontaneous atomic-scale magnetic skyrmion lattice in two dimensions, Nat. Phys. **7**, 713 (2011).

[8] C. Moreau-Luchaire, C. Moutafis, N. Reyren, J. Sampaio, C. A. F. Vaz, N. Van Horne, K. Bouzehouane, K. Garcia, C. Deranlot, P. Warnicke, P. Wohlhüter, J.-M. George, M. Weigand, J. Raabe, V. Cros, and A. Fert, Additive interfacial chiral interaction in multilayers for stabilization of small individual skyrmions at room temperature, Nat. Nanotechnol. **11**, 444 (2016).

[9] S. Woo, K. Litzius, B. Krüger, M.-Y. Im, L. Caretta, K. Richter, M. Mann, A. Krone, R. M. Reeve, M. Weigand, P. Agrawal, I. Lemesh, M.-A. Mawass, P. Fischer, M. Kläui, and G. S. D. Beach, Observation of room-temperature magnetic skyrmions and their current-driven dynamics in ultrathin metallic ferromagnets, Nat. Mater. **15**, 501 (2016).

[10] T. Dohi, S. DuttaGupta, S. Fukami, and H. Ohno, Formation and current-induced motion of synthetic antiferromagnetic skyrmion bubbles, Nat. Commun. **10**, 5153 (2019).

[11] D. A. Allwood, G. Xiong, C. C. Faulkner, D. Atkinson, D. Petit, and R. P. Cowburn, Magnetic domain-wall logic, Science **309**, 1688 (2005).

[12] M. Hayashi, L. Thomas, R. Moriya, C. Rettner, and S. S. P. Parkin, Current-controlled magnetic domain-wall nanowire shift register, Science **320**, 209 (2008).

[13] Z. Luo, A. Hrabec, T. P. Dao, G. Sala, S. Finizio, J. Feng, S. Mayr, J. Raabe, P. Gambardella, and L. J. Heyderman, Current-driven magnetic domain-wall logic, Nature (London) **579**, 214 (2020).

[14] J. Grollier, D. Querlioz, K. Y. Camsari, K. Everschor-Sitte, S. Fukami, and M. D. Stiles, Neuromorphic spintronics, Nat. Electron. **3**, 360 (2020).

[15] K. M. Song, J.-S. Jeong, B. Pan, X. Zhang, J. Xia, S. Cha, T.-E. Park, K. Kim, S. Finizio, J. Raabe, J. Chang, Y. Zhou, W. Zhao, W. Kang, H. Ju, and S. Woo, Skyrmion-based artificial synapses for neuromorphic computing, Nat. Electron. **3**, 148 (2020).

[16] N. Nagaosa and Y. Tokura, Topological properties and dynamics of magnetic skyrmions, Nat. Nanotechnol. **8**, 899 (2013).

[17] A. Fert, V. Cros, and J. Sampaio, Skyrmions on the track, Nat. Nanotechnol. **8**, 152 (2013).

[18] X. Zhang, M. Ezawa, and Y. Zhou, Magnetic skyrmion logic gates: conversion, duplication and merging of skyrmions, Sci. Rep. **5**, 9400 (2015).

[19] J. Zázvorka, F. Jakobs, D. Heinze, N. Keil, S. Kromin, S. Jaiswal, K. Litzius, G. Jakob, P. Virnau, D. Pinna, K. Everschor-Sitte, L. Rózsa, A. Donges, U. Nowak, and M. Kläui, Thermal skyrmion diffusion used in a reshuffler device, Nat. Nanotechnol. **14**, 658 (2019).

[20] Z. Luo, P. T. Dao, A. Hrabec, J. Vijayakumar, A. Kleibert, M. Baumgartner, E. Kirk, J. Cui, T. Savchenko, G. Krishnaswamy, J. L. Heyderman, and P. Gambardella, Chirally coupled nanomagnets, Science **363**, 1435 (2019).

[21] S.-H. Yang, Spintronics on chiral objects, Appl. Phys. Lett. **116**, 120502 (2020).

[22] C. Back, V. Cros, H. Ebert, K. Everschor-Sitte, A. Fert, M. Garst, T. Ma, S. Mankovsky, T. L. Monchesky, M. Mostovoy, N. Nagaosa, S. S. P. Parkin, C. Pfleiderer, N. Reyren, A. Rosch, Y. Taguchi, Y. Tokura, K. von Bergmann, and J. Zang, The 2020 skyrmionics roadmap, J. Phys. D: Appl. Phys. **53**, 363001 (2020).

[23] D.-H. Kim, M. Haruta, H.-W. Ko, G. Go, H.-J. Park, T. Nishimura, D.-Y. Kim, T. Okuno, Y. Hirata, Y. Futakawa, H. Yoshikawa, W. Ham, S. Kim, H. Kurata, A. Tsukamoto, Y. Shiota, T. Moriyama, S.-B. Choe, K.-J. Lee, and T. Ono, Bulk Dzyaloshinskii-Moriya interaction in amorphous ferrimagnetic alloys, Nat. Mater. **18**, 685 (2019).

[24] A. Fernández-Pacheco, E. Vedmedenko, F. Ummelen, R. Mansell, D. Petit, and R. P. Cowburn, Symmetry-breaking interlayer Dzyaloshinskii-Moriya interactions in synthetic antiferromagnets, Nat. Mater. **18**, 679 (2019).

[25] D.-S. Han, K. Lee, J.-P. Hanke, Y. Mokrousov, K.-W. Kim, W. Yoo, Y. L. W. van Hees, T.-W. Kim, R. Lavrijsen, C.-Y. You, H. J. M. Swagten, M.-H. Jung, and M. Kläui, Long-range chiral exchange interaction in synthetic antiferromagnets, Nat. Mater. **18**, 703 (2019).

[26] B. Göbel, I. Mertig, and O. A. Tretiakov, Beyond skyrmions: review and perspectives of alternative magnetic quasiparticles, Phys. Rep. **895**, 1 (2021).

[27] S.-G. Je, D.-H. Kim, S.-C. Yoo, B.-C. Min, K.-J. Lee, and S.-B. Choe, Asymmetric magnetic domain-wall motion by the Dzyaloshinskii-Moriya interaction, Phys. Rev. B **88**, 214401 (2013).

[28] A. Hrabec, N. A. Porter, A. Wells, M. J. Benitez, G. Burnell, S. McVitie, D. McGrouther, T. A. Moore, and C. H. Marrows, Measuring and tailoring the Dzyaloshinskii-Moriya interaction in perpendicularly magnetized thin films, Phys. Rev. B **90**, 020402 (2014).

[29] J. Torrejon, J. Kim, J. Sinha, S. Mitani, M. Hayashi, M. Yamanouchi, and H. Ohno, Interface control of the magnetic chirality in CoFeB/MgO heterostructures with heavy-metal underlayers, Nat. Commun. **5**, 4655 (2014).

[30] R. Lavrijsen, D. M. F. Hartmann, A. van den Brink, Y. Yin, B. Barcones, R. A. Duine, M. A. Verheijen, H. J. M. Swagten, and B. Koopmans, Asymmetric magnetic bubble expansion under in-plane field in Pt/Co/Pt: Effect of interface engineering, Phys. Rev. B **91**, 104414 (2015).

[31] D.-S. Han, N.-H. Kim, J.-S. Kim, Y. Yin, J.-W. Koo, J. Cho, S. Lee, M. Kläui, H. J. M. Swagten, B. Koopmans, and C.-Y. You, Asymmetric hysteresis for probing Dzyaloshinskii-Moriya interaction, Nano Lett. **16**, 4438 (2016).

[32] C.-F. Pai, M. Mann, A. J. Tan, and G. S. D. Beach, Determination of spin torque efficiencies in heterostructures with perpendicular magnetic anisotropy, Phys. Rev. B **93**, 144409 (2016).

[33] S. Kim, P.-H. Jang, D.-H. Kim, M. Ishibashi, T. Taniguchi, T. Moriyama, K.-J. Kim, K.-J. Lee, and T. Ono, Magnetic droplet nucleation with a homochiral Néel domain wall, Phys. Rev. B **95**, 220402 (2017).

[34] K. Di, V. L. Zhang, H. S. Lim, S. C. Ng, M. H. Kuok, J. Yu, J. Yoon, X. Qiu, and H. Yang, Direct Observation of the Dzyaloshinskii-Moriya Interaction in a Pt/Co/Ni Film, Phys. Rev. Lett. **114**, 047201 (2015).

[35] J. Cho, N.-H. Kim, S. Lee, J.-S. Kim, R. Lavrijsen, A. Solignac, Y. Yin, D.-S. Han, N. J. J. van Hoof, H. J. M. Swagten, B. Koopmans, and C.-Y. You, Thickness dependence of the interfacial Dzyaloshinskii-Moriya interaction in inversion symmetry broken systems, Nat. Commun. **6**, 7635 (2015).

[36] H. T. Nembach, J. M. Shaw, M. Weiler, E. Jué, and T. J. Silva, Linear relation between Heisenberg exchange and interfacial Dzyaloshinskii-Moriya interaction in metal films, Nat. Phys. **11**, 825 (2015).

[37] S. Emori, E. Martinez, K.-J. Lee, H.-W. Lee, U. Bauer, S.-M. Ahn, P. Agrawal, D. C. Bono, and G. S. D. Beach, Spin Hall torque magnetometry of Dzyaloshinskii domain walls, Phys. Rev. B **90**, 184427 (2014).

[38] D.-Y. Kim, M.-H. Park, Y.-K. Park, J.-S. Kim, Y.-S. Nam, D.-H. Kim, S.-G. Je, H.-C. Choi, B.-C. Min, and S.-B. Choe, Chirality-induced antisymmetry in magnetic domain wall speed, NPG Asia Mater. **10**, e464 (2018).

[39] C. O. Avci, E. Rosenberg, L. Caretta, F. Büttner, M. Mann, C. Marcus, D. Bono, C. A. Ross, and G. S. D. Beach, Interface-driven chiral magnetism and current-driven domain walls in insulating magnetic garnets, Nat. Nanotechnol. **14**, 561 (2019).

[40] J. Sinova, S. O. Valenzuela, J. Wunderlich, C. H. Back, and T. Jungwirth, Spin Hall effects, Rev. Mod. Phys. **87**, 1213 (2015).

[41] R. Ramaswamy, J. M. Lee, K. Cai, and H. Yang, Recent advances in spin-orbit torques: Moving towards device applications, Appl. Phys. Rev. **5**, 031107 (2018).

[42] A. Manchon, J. Železný, I. M. Miron, T. Jungwirth, J. Sinova, A. Thiaville, K. Garello, and P. Gambardella, Current-induced spin-orbit torques in ferromagnetic and antiferromagnetic systems, Rev. Mod. Phys. **91**, 035004 (2019).

[43] D.-H. Kim, D.-Y. Kim, S.-C. Yoo, B.-C. Min, and S.-B. Choe, Universality of Dzyaloshinskii-Moriya interaction effect over domain-wall creep and flow regimes, Phys. Rev. B **99**, 134401 (2019).

[44] D.-Y. Kim, N.-H. Kim, Y.-K. Park, M.-H. Park, J.-S. Kim, Y.-S. Nam, J. Jung, J. Cho, D.-H. Kim, J.-S. Kim, B.-C. Min, S.-B. Choe, and C.-Y. You, Quantitative accordance of Dzyaloshinskii-Moriya interaction between domain-wall and spin-wave dynamics, Phys. Rev. B **100**, 224419 (2019).

[45] M. Mann and G. S. D. Beach, Reduction of in-plane field required for spin-orbit torque magnetization reversal by insertion of Au spacer in Pt/Au/Co/Ni/Co/Ta, APL Mater. **5**, 106104 (2017).

[46] J. Cao, Y. Chen, T. Jin, W. Gan, Y. Wang, Y. Zheng, H. Lv, S. Cardoso, D. Wei, and W. S. Lew, Spin orbit torques induced magnetization reversal through asymmetric domain wall propagation in Ta/CoFeB/MgO structures, Sci. Rep. **8**, 1355 (2018).

[47] D. Khadka, S. Karayev, and S. X. Huang, Dzyaloshinskii-Moriya interaction in Pt/Co/Ir and Pt/Co/Ru multilayer films, J. Appl. Phys. **123**, 123905 (2018).

[48] Y. Ishikuro, M. Kawaguchi, N. Kato, Y.-C. Lau, and M. Hayashi, Dzyaloshinskii-Moriya interaction and spin-orbit torque at the Ir/Co interface, Phys. Rev. B **99**, 134421 (2019).

[49] L. Liu, X. Zhao, W. Liu, Y. Song, X. Zhao, and Z. Zhang, Influence of rare earth metal Ho on the interfacial Dzyaloshinskii-Moriya interaction and spin torque efficiency in Pt/Co/Ho multilayers, Nanoscale **12**, 12444 (2020).

[50] T.-Y. Chen, W.-B. Liao, T.-Y. Chen, T.-Y. Tsai, C.-W. Peng, and C.-F. Pai, Current-induced spin–orbit torque efficiencies in W/Pt/Co/Pt heterostructures, Appl. Phys. Lett. **116**, 072405 (2020).

[51] S. Ding, L. Baldrati, A. Ross, Z. Ren, R. Wu, S. Becker, J. Yang, G. Jakob, A. Brataas, and M. Kläui, Identifying the origin of the nonmonotonic thickness dependence of spin-orbit torque and interfacial Dzyaloshinskii-Moriya interaction in a ferrimagnetic insulator heterostructure, Phys. Rev. B **102**, 054425 (2020).

[52] T. Dohi, S. DuttaGupta, S. Fukami, and H. Ohno, Reversal of domain wall chirality with ferromagnet thickness in W/(Co)FeB/MgO systems, Appl. Phys. Lett. **114**, 042405 (2019).

[53] S. Pizzini, J. Vogel, S. Rohart, L. D. Buda-Prejbeanu, E. Jué, O. Boulle, I. M. Miron, C. K. Safeer, S. Auffret, G. Gaudin, and A. Thiaville, Chirality-Induced Asymmetric Magnetic Nucleation in Pt/Co/AlO_x Ultrathin Microstructures, Phys. Rev. Lett. **113**, 047203 (2014).

[54] A. Thiaville, S. Rohart, É. Jué, V. Cros, and A. Fert, Dynamics of Dzyaloshinskii domain walls in ultrathin magnetic films, Europhys. Lett. **100**, 57002 (2012).

[55] S. Jaiswal, K. Litzius, I. Lemesh, F. Büttner, S. Finizio, J. Raabe, M. Weigand, K. Lee, J. Langer, B. Ocker, G. Jakob, G. S. D. Beach, and M. Kläui, Investigation of the Dzyaloshinskii-Moriya interaction and room temperature skyrmions in W/CoFeB/MgO thin films and microwires, Appl. Phys. Lett. **111**, 022409 (2017).

[56] X. Ma, G. Yu, C. Tang, X. Li, C. He, J. Shi, K. L. Wang, and X. Li, Interfacial Dzyaloshinskii-Moriya Interaction: Effect of 5d Band Filling and Correlation with Spin Mixing Conductance, Phys. Rev. Lett. **120**, 157204 (2018).

[57] M. Vaňatka, J.-C. Rojas-Sánchez, J. Vogel, M. Bonfim, M. Belmeguenai, Y. Roussigné, A. Stashkevich, A. Thiaville, and S. Pizzini, Velocity asymmetry of Dzyaloshinskii domain walls in the creep and flow regimes, J. Phys.: Condens. Matter **27**, 326002 (2015).

[58] M. Heide, G. Bihlmayer, and S. Blügel, Dzyaloshinskii-Moriya interaction accounting for the orientation of magnetic domains in ultrathin films: Fe/W(110), Phys. Rev. B **78**, 140403(R) (2008).

[59] J.-S. Kim, Y.-S. Nam, D.-Y. Kim, Y.-K. Park, M.-H. Park, and S.-B. Choe, Comparison between spin-orbit torques measured by domain-wall motions and harmonic measurements, AIP Adv. **8**, 056009 (2018).

[60] S.-W. Jung, W. Kim, T.-D. Lee, K.-J. Lee, and H.-W. Lee, Current-induced domain wall motion in a nanowire with perpendicular magnetic anisotropy, Appl. Phys. Lett. **92**, 202508 (2008).

[61] N. Ichikawa, T. Dohi, A. Okada, H. Sato, S. Fukami, and H. Ohno, Non-linear variation of domain period under electric field in demagnetized CoFeB/MgO stacks with perpendicular easy axis, Appl. Phys. Lett. **112**, 202402 (2018).

[62] N. Sato, R. M. White, and S. X. Wang, Effect of annealing on exchange stiffness of ultrathin CoFeB film with perpendicular magnetic anisotropy, Appl. Phys. Lett. **108**, 152405 (2016).

[63] T. Dohi, S. Kanai, F. Matsukura, and H. Ohno, Electric-field effect on spin-wave resonance in a nanoscale CoFeB/MgO magnetic tunnel junction, Appl. Phys. Lett. **111**, 072403 (2017).

[64] J. Cho, S. Miwa, K. Yakushiji, S. Tamaru, H. Kubota, A. Fukushima, S. Fujimoto, E. Tamura, C.-Y. You, S. Yuasa, and Y. Suzuki, Spin-wave eigenmodes in single disk-shaped FeB nanomagnet, Phys. Rev. B **94**, 184411 (2016).

[65] C. J. Safranski, Y.-J. Chen, I. N. Krivorotov, and J. Z. Sun, Material parameters of perpendicularly magnetized tunnel junctions from spin torque ferromagnetic resonance techniques, Appl. Phys. Lett. **109**, 132408 (2016).

[66] T. Devolder, J.-V. Kim, L. Nistor, R. Sousa, B. Rodmacq, and B. Diény, Exchange stiffness in ultrathin perpendicularly magnetized CoFeB layers determined using the spectroscopy of electrically excited spin waves, J. Appl. Phys. **120**, 183902 (2016).

[67] Y.-K. Park, D.-Y. Kim, J.-S. Kim, Y.-S. Nam, M.-H. Park, H.-C. Choi, B.-C. Min, and S.-B. Choe, Experimental observation of the correlation between the interfacial Dzyaloshinskii-Moriya interaction and work function in metallic magnetic trilayers, NPG Asia Mater. **10**, 995 (2018).

[68] J.-C. Rojas-Sánchez, P. Laczkowski, J. Sampaio, S. Collin, K. Bouzehouane, N. Reyren, H. Jaffrès, A. Mougin, and J.-M. George, Perpendicular magnetization reversal in $Pt/[Co/Ni]_3/Al$ multilayers via the spin Hall effect of Pt, Appl. Phys. Lett. **108**, 082406 (2016).

[69] O. Boulle, S. Rohart, L. D. Buda-Prejbeanu, E. Jué, I. M. Miron, S. Pizzini, J. Vogel, G. Gaudin, and A. Thiaville, Domain Wall Tilting in the Presence of the Dzyaloshinskii-Moriya Interaction in Out-of-Plane Magnetized Magnetic Nanotracks, Phys. Rev. Lett. **111**, 217203 (2013).

[70] D.-Y. Kim, M.-H. Park, Y.-K. Park, J.-S. Kim, Y.-S. Nam, H.-S. Hwang, D.-H. Kim, S.-G. Je, B.-C. Min, and S.-B. Choe, Magnetic domain-wall tilting due to domain-wall speed asymmetry, Phys. Rev. B **97**, 134407 (2018).

[71] M. Kawaguchi, K. Tanabe, K. Yamada, T. Sawa, S. Hasegawa, M. Hayashi, and Y. Nakatani, Determination of the Dzyaloshinskii-Moriya interaction using pattern recognition and machine learning, Npj Comput. Mater. **7**, 20 (2021).

[72] J. Moritz, B. Dieny, J. P. Nozières, Y. Pennec, J. Camarero, and S. Pizzini, Experimental evidence of a $1/H$ activation law in nanostructures with perpendicular magnetic anisotropy, Phys. Rev. B **71**, 100402 (2005).